Evaluation of Mass Transport Properties of the Advanced Medical-Interesting Porous Solids

KAREL SOUKUP, VLADIMÍR HEJTMÁNEK, AND OLGA ŠOLCOVÁ
Institute of Chemical Process Fundamentals of the ASCR, v. v. i.
Rozvojová 135, CZ-165 02 Prague 6
CZECH REPUBLIC
soukup@icpf.cas.cz http://www.icpf.cas.cz/en/user/soukup

Abstract: - Investigation has been focused on detailed determination of the mass transport properties of novel biomaterials with unique properties for clinical applications consisted of the polymeric electrospun membranes (chitosan and polyurethane) and bone-like hydroxyapatite. Transport characteristics were determined both in the gaseous and the liquid systems by combination of Graham's diffusion cell and an inverse liquid chromatography technique. The optimum transport parameters for chitosan and polyurethane nanofibrous membranes were found as follows: $\langle r \rangle_\psi$ = 61.5 nm, ψ =0.130 and $\langle r \rangle_\psi$ = 61.2 nm, ψ = 0.165, respectively. Furthermore, based on comparison of the transport parameters with textural characteristics was concluded that the most significance role in the mass transport process play a fraction of pores with radii between 370 and 470 nm. Effective diffusion coefficients (5.92×10^{-17} and 6.54×10^{-17} cm^2/s) for two polystyrene samples with different molecular weight (1000 and 100,000, respectively) in cyclohexane were determined from the responses of a chromatographic column packed with the bone-like hydroxyapatite.

Key-Words: -Biocompatible material; Electrospun nanofibrous membrane; Chitosan; Polyurethane; Bone-like hydroxyapatite; Graham's diffusion cell; Inverse liquid chromatography; Transport characteristics

1 Introduction

The recent trend in biomedical research is focused on advanced biomaterials with unique highly selective properties for clinical applications. Currently, the great interest of many research groups is focused on the use of biocompatible bone-like hydroxyapatite [1] or biocompatible electrospun nanofibers [2].

Biocompatible and biodegradable hydroxyapatite ($Ca_{10}(PO_4)_6(OH)_2$) represents one of the major constituents of the inorganic components of human hard tissues, bones, tendons and teeth [3]. Generally, it shows an excellent biocompatibility not only with the hard tissue but also with the soft tissue. Hydroxyapatite is capable of integrating biologically when directly implanted into a bone defect; furthermore, it is osteoconductive, nontoxic, noninflammatory, nonimmunogenic agent and bioactive, i.e. ability to form a direct chemical bond with living tissues [1].

Biomedical field is one of the important application areas utilizing nanofibers prepared by the electrospinning technique [4]. Nanofiber research in biomedical engineering consists of tissue engineering, wound dressing, affinity membrane and drug delivery systems [2].

The knowledge of transport parameters of the porous biocompatible materials is decisive for the exact description of the mass transport kinetics in pores. Experimental methods based on the direct mass transport measurements can be, in principle, divided according to the measurement conditions into two groups—steady-state and dynamic. In general, most studies based on the steady-state gas transport measurements use the technique developed by Wicke and Kallenbach[5] and many subsequent modifications of this method, as demonstrated by numerous contributions in literature [6–10]. Important modification is represented by a Graham's diffusion cell [10]. The main advantage of this arrangement is the relative simplicity of the experimental equipment, in contrast to the classic Wicke-Kallenbach cell which needs to analyze the output gas streams from the diffusion cell.

Inverse chromatography [11] is a typical representative of techniques based on the transport measurements under dynamic conditions. Unlike in analytical chromatography the stationary phase is the investigated solid sample and the gas or liquid mobile phase acts as a probe molecule. The main advantages of this arrangement include the ability to work with peculiarly (non-cylindrical) shaped samples as well as with powder materials.

2 Problem Formulation

The proposed study is focused on determination of the mass transport properties of the medical-interesting porous solids consist of the electrospun nanofibers based on chitosan (CS), polyurethane (PU), and bone-like hydroxyapatite (HA). Corresponding transport characteristics were determined in the both gas/solid and liquid/solid systems based on measurements including combination of Graham's diffusion cell and the inverse liquid chromatography method.

2.1 Electrospinning

Biocompatible nanofibrous membranes based both on chitosan and polyurethane were prepared from the fresh solution by electrospinning technique. The used experimental apparatus for nanofibrous membranes production (Elmarco, Czech Republic) depicted in Fig. 1 involved the steel rotation spinning electrode with the needles and the steel cylinder as the collecting electrode. The electric voltage 75 kV (DC power supply, Matsusada Precision, Japan), temperature between 20–25 °C, relative humidity between 25–35% and the electrode spinning rate 8 min^{-1} were used for the electrospinning process.

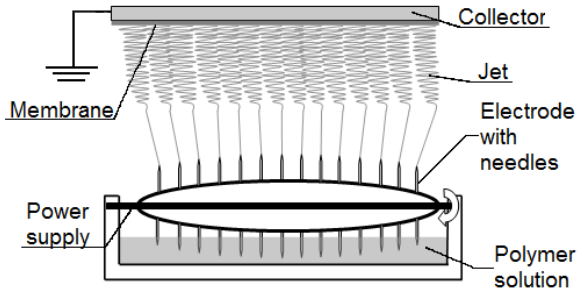

Fig. 1 Electrospinning setup

2.2 Textural Analysis

Textural properties of the both chitosan and polyurethane membranes as well as hydroxyapatite sample were evaluated by using standard textural methods included the high-pressure mercury porosimetry (AutoPore III, Micromeritics, USA), physical adsorption of nitrogen (ASAP 2050, Micromeritics, USA) at 77 K and helium pycnometry (AccuPyc 1330, Micromeritics, USA). To guarantee the precision of the obtained data purities of used nitrogen and helium (Linde Gas, Czech Republic) were 99.9995%. Before analysis all samples were dried at 50 °C (nanofibrous membrane) or 300 °C (hydroxyapatite) for 24 hours in vacuum (0.1 Pa).

2.3 Gas Diffusion Measurements

Gas diffusion measurements with chitosan and polyurethane membrane were performed in Graham's diffusion cell.

Sample of a circle shape (diameters equal to 5 mm) were prepared either from the parent electrospun mats by using a die cutting tool. The sample test area clamped in the impermeable disc exposed a circular area of 0.196 cm^2 to the upper and lower gas streams. All counter-current gas diffusion measurements had to be performed very carefully owing to soft and easily deformable structure of membranes.

During the gas diffusion measurements gases flowed steadily through the upper and lower cell chambers until the steady-state was established. Thereafter, the gas inlet and outlet in one of the cell chambers (typically the lower chamber) were closed and the net volumetric diffusion flux was determined by a digital bubble flowmeter (Optiflow HFM 570, Agilent Technologies, USA) connected to the bottom cell compartment. The heavier gas was always fed into the upper cell compartment. Three not adsorbing gases included nitrogen, helium and argon (99.99% purity, Linde Gas, Czech Republic) were used for the diffusion tests.

2.3.1 Transport Parameters Evaluation

Isobaric gas diffusion transport taking place in pores during the gas diffusion measurements with the nanofibrous membrane was modeled by means of the Mean Transport-Pore Model (MTPM) approach [12] based on the constitutive Maxwell-Stefan equation. In this model description the transport-pores are visualized as cylindrical capillaries with radii distributed around the integral mean transport-pore radius, $\langle r \rangle$. MTPM takes also into account their porosity, ε_t, and tortuosity, q_t (parameter $\psi = \varepsilon_t / q_t$). For an n-component gas mixture and one dimensional purely diffusion flux the modified Maxwell-Stefan diffusion equation can be formulated as:

$$-c\frac{\mathrm{d}y_i}{\mathrm{d}x} = \frac{N_i^d}{D_i^k} + \sum_{\substack{j=1 \\ j\neq i}}^{n} \frac{y_j N_i^d - y_i N_j^d}{D_{ij}^m},\ i = 1,..,n \qquad (1)$$

where c denotes the total molar gas concentration, y_i is the mole fraction of component i, x stands for the length coordinate in the diffusion direction and N_i^d is the molar diffusion flux density of component i per unit total cross-section of the porous solid, D_i^k represents the effective Knudsen diffusion

coefficient and D_{ij}^{m} denotes the effective binary bulk diffusion coefficient of the pair *i–j*.
The effective Knudsen diffusivity of component *i* can be expressed as:

$$D_i^k = \langle r \rangle \psi K_i \quad (2)$$

where K_i stands for:

$$K_i = \frac{2}{3}\sqrt{\frac{8R_gT}{\pi M_i}} \quad (3)$$

where R_g is the gas constant, T temperature and M_i the molecular weight of component *i*. The effective binary bulk diffusion coefficient of the pair *i–j* can be defined as follows:

$$D_{ij}^{m} = \psi \mathsf{D}_{ij}^{m} \quad (4)$$

with the binary bulk diffusion coefficient D_{ij}^{m}.

Numerical solution of Eq. (1) as well as evaluation of transport parameters can be found elsewhere [8].

2.4 Inverse Liquid Chromatography

Transport properties of the biocompatible bone-like hydroxyapatite obviously promoting adhesion and proliferation of the bone forming cells (osteoblasts) were characterized by means of the effective diffusion coefficients. Polystyrenes which are able to replace real biopolymers (amino acids, proteins, etc.), in our case like model compounds used, due to possibility to control molar weight in a wide range order of magnitude were used as appropriate tracers.

All experiments in the liquid/solid system were carried out in the arrangement of adapted version of the inverse liquid chromatography. During experiment, the mobile phase consisted of cyclohexane (HPLC grade, Carl Roth, Germany) flows through the hydroxyapatite sample. Column was perturbed by flushing of sampling loop (volume 20 μL) filled with diluted tracer of solute (polystyrene samples with average relative molecular weight of 1000 or 100,000, analytical standard, Fluka, Sigma-Aldrich Czech Republic). The solute concentration in the column outlet was monitored by a refractometry detector (Perkin Elmer Instruments, USA).

2.4.1Effective Diffusion Coefficients Evaluation

For the exact description of phenomena taking place inside chromatographic column the Kubín-Kučera model [11,12] including convection, external and intraparticle diffusion, axial dispersion and the effects of small ideally mixed volumes at inlet and outlet of the column [15] was utilized as follows:

$$E\frac{\partial^2 c}{\mathrm{d}x^2} - v\frac{\partial c}{\partial x} - \frac{\partial c}{\partial t} - \frac{3D_{eff}}{R}\frac{(1-\alpha)}{\alpha}\left(\frac{\partial c_p}{\partial r}\right)_{r=R} = 0 \quad (5)$$

where E represents the axial dispersion coefficient, c is the polystyrene concentration in the intraparticle space, v is the cyclohexane interstitial linear velocity, t is the column retention time, D_{eff} denotes the effective diffusion coefficient, R is the radius of the primary hydroxyapatite particles, α is the column void fraction, c_p is the polystyrene concentration in pores and finally, r denotes the coordinate.

Evaluation of the effective diffusion coefficients of tested hydroxyapatite samples was based on matching of column responses (chromatographic peaks) in the time domain. More detail information concerning numerical solution can be found in [15].

3 Problem Solution

3.1 Preparation of Biodegradable Materials

Generally, any minor changes both in the polymeric solution properties (viscosity, concentration, conductivity, etc.) and electrospinning parameters (electric voltage applied, distance and shape of the electrodes, etc.) can result in significant variations in the final morphology of nanofibrous membranes. Thus, a special effort was devoted to the optimization of all electrospinning parameters to prepare bead-free fibers with uniform distribution of the fiber diameters.

Chitosan (low molecular weight, Sigma-Aldrich, powder) and polyvinyl alcohol (Mowiol 10-98, Kuraray, powder) with the weight ratio 1:10 were dissolved in a mixture of acetic acid (PentaChemikalie, Czech Republic, p.a. grade) and deionized water (conductivity lower than 2 μs/cm) with the volume ratio 1:1. The weight concentration of polymers was adjusted to 14.5% (w/v) and the specific electric conductivity to 1100 μS/cm by adding sodium chloride to the prepared polymeric solution, which was found as optimum for the electrospinning process.

Polyurethane solution was prepared by dissolving parent polyurethane granulate (Desmopan DP 2590A, Bayer Material Science, Germany) in mixed methylisobutylketone and dimethylformamide (volume ratio 1:3), the weight concentration was adjusted to 15.5 % (w/v) and the

electric conductivity to 150 μS/cm by using tetraethylamonium-bromide. Final solution was stirred at 50 °C for 12 h and thereafter cooled down to the laboratory temperature after complete dissolving.

Nanopowder of hydroxyapatite with the particle size less than 200 nm corresponding to biocompatible grade was purchased from Sigma-Aldrich.

3.2 SEM Image Analysis

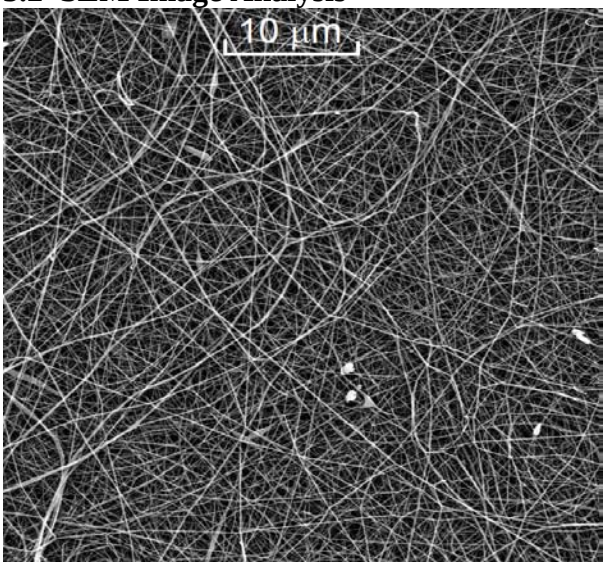

Fig. 2 SEM micrograph of chitosan

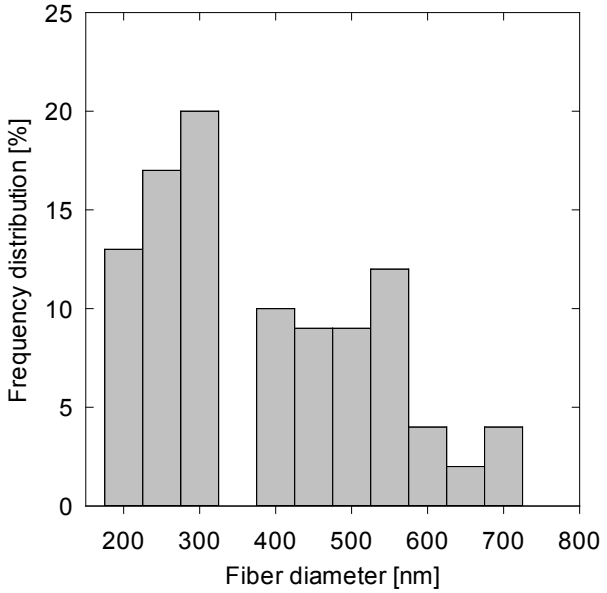

Fig. 3 Fiber diameter distribution for chitosan

Based on the systematic study on the effect of electrospinning conditions on the bead-free chitosan and polyurethane nanofibrous membranes the optimal conditions were found and spinning solution concentration was recognized as the main parameter (the higher viscosity of the polymeric solution the lower number of beads). SEM micrographs in Figs. 2 and 4 show typical morphology of the prepared electrospun chitosan and polyurethane membranes. It can be clearly recognized that nanofibrous membranes comprise predominantly bead-free uniform fibers typically oriented randomly over each other. Based on the SEM micrographs, the statistical distribution of the diameter was calculated from at least 100 individual fibers. Computed histograms are given in Figs. 3 and 5. It was found rather broader fiber diameter distributions with fiber diameters between 200 nm and 700 nm for the chitosan membranes. Contrary, polyurethane revealed uniform fibers with generally smaller diameters ranging from 50 nm to 450 nm.

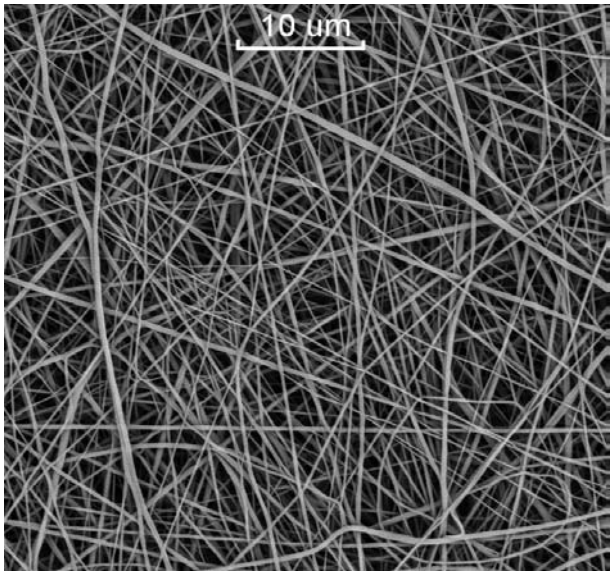

Fig. 4 SEM micrograph of polyurethane

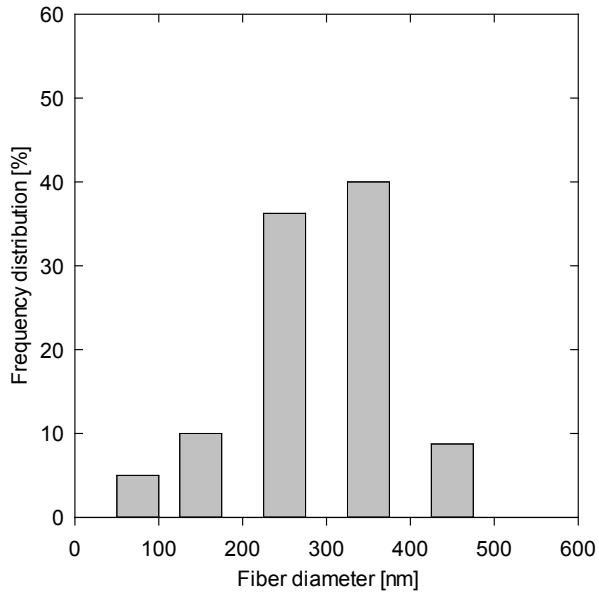

Fig. 5 Fiber diameter distribution for polyurethane

Through Fig. 6 depicting SEM micrograph of the hydroxyapatite sample can be recognized the bigger secondary aggregated particles of hydroxyapatite; however, the size of the primary particles declared by the producer is approximately 200 nm.

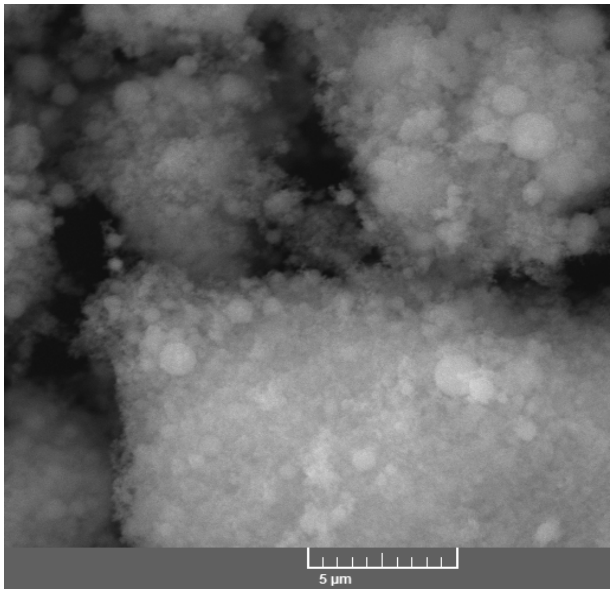

Fig 6 SEM micrograph of biocompatible hydroxyapatite

3.3 Textural Study

The basic textural properties including the BET surface area (S_{BET}), the total intrusion volume (V_{intr}), the skeletal (ρ_{He}) and apparent (ρ_{Hg}) densities and the porosity (ε) of the tested nanofibrous membranes as well as hydroxyapatite are listed in Table 1.

Table 1 Textural properties of tested samples

Sample	S_{BET} [m^2/g]	V_{intr} [cm^3/g]	ρ_{He} [g/cm^3]	ρ_{Hg} [g/cm^3]	ε [–]
CS	14.5	3.61	1.19	0.22	0.81
PU	2.8	1.07	1.12	0.52	0.54
HA	19.6	1.06	2.94	2.06	0.30

Results, as illustrated in Table 1, suggest that chitosan nanofibers show the highest total porosity and the lowest apparent density. On the other hand, polyurethane membrane reveals rather low BET surface area but the highest pore volume of all samples. Hydroxyapatite shows the highest magnitude of the inner surface area and the lowest total porosity.

Pore-size distribution functions (PSD) evaluated from the high-pressure mercury porosimetry (for both chitosan and polyurethane samples) and physical adsorption of nitrogen (hydroxyapatite sample) are presented through Figs. 7–9. It can be recognized that chitosan membrane with the prevailing pore radius corresponding to 130 nm shows rather narrower peak on PSD. For the PSD of polyurethane sample a broad peak with a maximum of 456 nm was confirmed. On the other hand, the hydroxyapatite sample reveals obviously narrower peak with the prevailing pore radius of 30 nm.

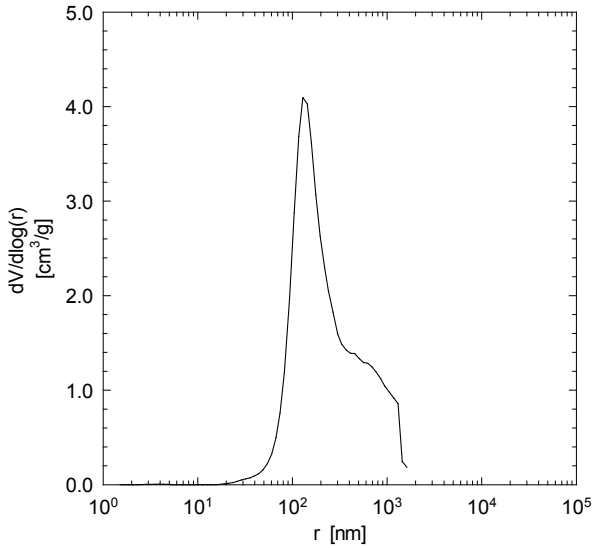

Fig. 7 Pore-size distribution curve obtained from high-pressure mercury porosimetry for chitosan

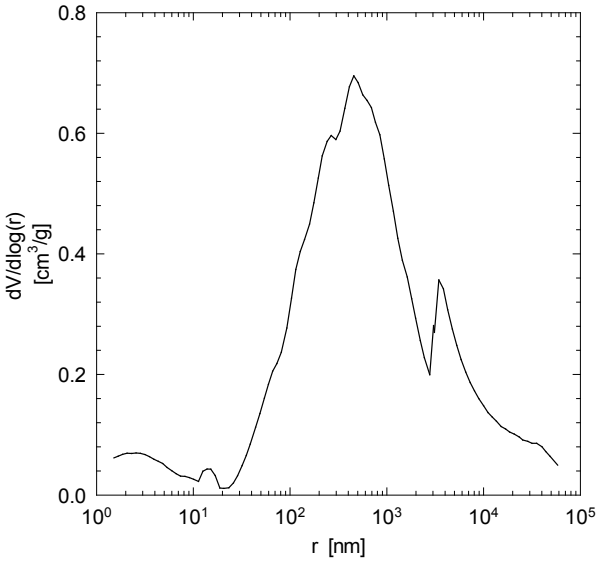

Fig. 8 Pore-size distribution curve obtained from high-pressure mercury porosimetry for polyurethane

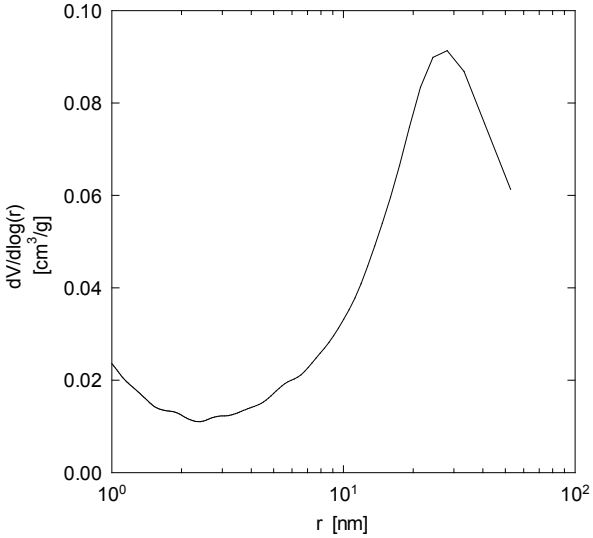

Fig. 9 Pore-size distribution curve obtained from physical adsorption of nitrogen for hydroxyapatite

3.4 Determination of transport parameters of Electrospun Nanofibrous Membranes

The net diffusion volumetric fluxes were determined for all possible combinations of the four used inert gases (Ar, N_2, He, and H_2). The following gas pairs were used: Ar/N_2, Ar/He, Ar/H_2, N_2/He, N_2/H_2, and He/H_2. In addition, six ternary diffusion measurements were also performed with the following gas mixtures: Ar/(N_2 + He), Ar/(N_2 + H_2), (Ar + H_2)/He, (Ar + N_2)/He, (Ar + He)/H_2, and (He + N_2)/H_2. The diffusion experimental data sets include 30 points (every experimental point was three times repeated, the mean values were taken to the transport parameter computation) both for binary cases (pure gases in both chambers of the diffusion cell) and ternary cases (pure gas in one chamber and binary mixture of two other gases in the opposite chamber).

The optimum transport parameters found both for chitosan and polyurethane samples are summarized in Table 2.

Table 2 Transport parameters of nanofibrous mats

Sample	$\langle r\rangle\psi$ [nm]	ψ [–]	$\langle r\rangle$ [nm]
Chitosan	61.5	0.130	473
Polyurethane	61.2	0.165	371

The mean transport-pore radii, $\langle r\rangle$, listed in Table 2 were calculated according to $(\langle r\rangle\psi)/\psi$. Figs. 10 and 11 compare the mean transport-pore radii with the pore-size distribution obtained from the high-pressure mercury porosimetry. It appears that for polyurethane membrane the mean transport-pore radius agrees well with the maximum of PSD (456 nm). On the other hand, for chitosan membrane the mean transport-pore radius is positioned outside the peak maximum (130 nm) closer to area corresponding to the wider pores. It follows that the gas transport takes place rather through the wider pores, which is in physical agreement with the concept of the path of least resistance (the physical pathway that provides the least mass transport resistance). The role of narrower pores depends on their size and total amount.

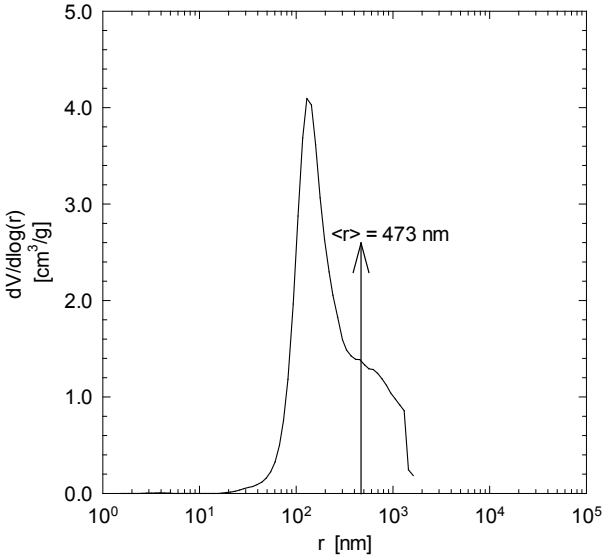

Fig. 10 Comparison of pore-size distribution (solid line) with the mean transport pore radius ($\langle r\rangle$, arrow) for chitosan membrane

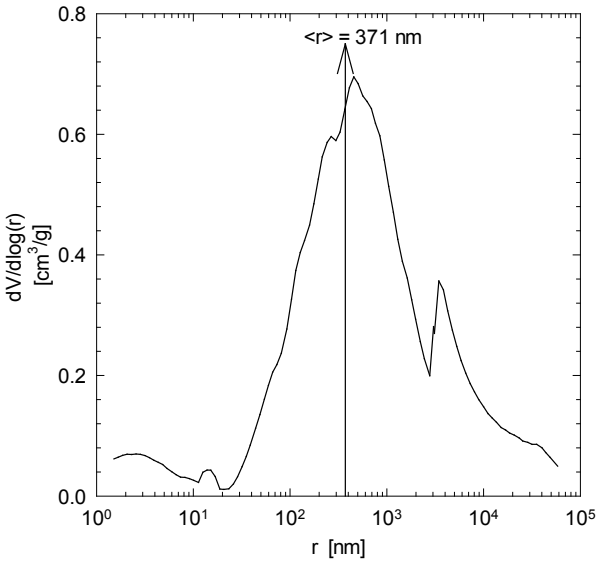

Fig. 11 Comparison of pore-size distribution (solid line) with the mean transport pore radius ($\langle r\rangle$, arrow) for polyurethane membrane

3.5 Determination of Effective Diffusion Coefficients in Liquid System

The effective diffusion coefficients, D_{eff}, were evaluated from fitted diffusion time constant according to: $t_{dif} = R^2\varepsilon S/D_{eff}$ where R denotes particle radius, ε is the hydroxyapatite porosity, S the steric factor (partition coefficient). The steric factor is defined as the ratio between hydraulic (Stokes) diameter of polystyrene molecule, d_h, and pore diameter of hydroxyapatite material, d_p, according to $S = 1–(d_h/d_p)^2$. Hydraulic diameters for polystyrenes with relative molecular weight of 1000 and 100,000 were determined using the correlation equation given in [16] and the resulting values are summarized in Table 3.

The bulk binary diffusion coefficients, D_{bulk}, of the polystyrene/cyclohexane pairs summarized in Table 3 were calculated according to the empirical relation given in [17].

Fig. 12 demonstrates a very good fit between experimental data and the calculated chromatographic response based on the optimized model parameters.

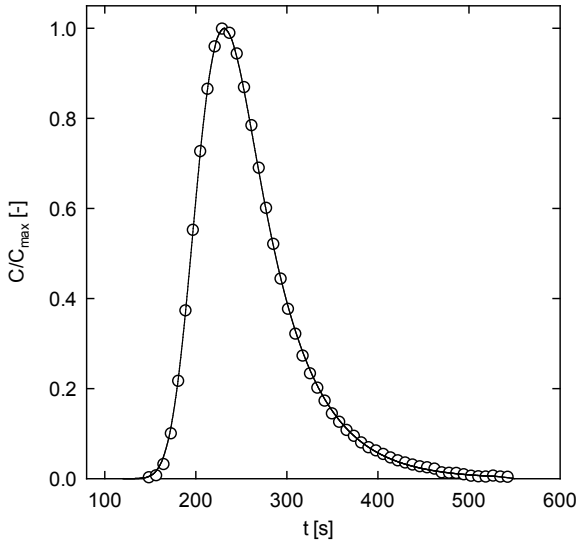

Fig. 12 Response curve for polystyrene tracer (M_w = 100,000) in cyclohexane (F = 300 μL/min) on hydroxyapatite. Experimental (°), calculated (—)

In Fig. 13 the chromatographic peaks for polystyrene solutes with different molecular weights are compared. It can be clearly seen that polystyrene samples with the larger molecular weight (M_w = 100,000) shows shorter retention time compared to polystyrene with the lower molecular weight (M_w = 1000). The observed difference in retention times corresponds to expectation that short-chain polystyrene (M_w = 1000) will penetrate deeper to the pore system and will be more retained in comparison with the long-chain polystyrene (M_w = 100,000).

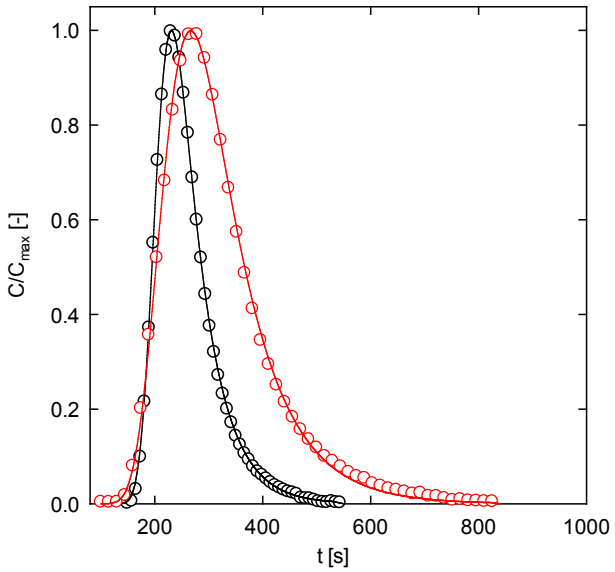

Fig. 13 Comparison of response curves for polystyrene tracers with different molecular weights. M_w = 100,000 – black marks and M_w = 1000 – red marks

The effective diffusion coefficients for polystyrene solutes with relative molecular weight 1000 and 100,000 in cyclohexane on hydroxyapatite are summarized in Table 3. It appears from comparison of the binary bulk diffusivities with the effective counterparts that hindered diffusion of the large molecules generally plays a key role for overall transport rates of solutes taking place inside biocompatible hydroxyapatite. However, the effective diffusivities for tested polystyrenes were independent on the length of their chain. The main reason lies in the hydraulic diameters of the both polystyrenes which were significantly smaller compared to diameters of the pores inside hydroxyapatite (prevailing pore diameter 60 nm in hydroxyapatite in comparison with 1.4 and 13.9 nm corresponding to the hydraulic diameters of polystyrenes).

Table 3 Diffusion coefficients of polystyrene/cyclohexane (F = 300 μL/min) on hydroxyapatite

Mw [–]	d_h [nm]	t_{dif} [g/cm^3]	D_{bulk}x10^{10} [cm^2/s]	D_{eff}x10^{17} [cm^2/s]
1000	1.4	48.4	3.23	5.92
100,000	13.9	27.1	0.32	6.54

4 Conclusion

Transport characteristics were determined in the gas/solid as well in the liquid/solid systems by combination of Graham's diffusion cell and the inverse liquid chromatography technique. Based on the isothermal counter-current gas diffusion measurements carried out in Graham's diffusion cell the optimum transport parameters for chitosan and polyurethane nanofibrous membranes were found as follows: $\langle r \rangle_\psi$ = 61.5 nm, ψ = 0.130 and $\langle r \rangle_\psi$ = 61.2 nm, ψ = 0.165, respectively. The obtained transport parameters were compared with characteristics evaluated from the standard textural analyses. It was found that the most significant role in the mass transport process play fraction of pores with radii between 370 and 470 nm.

Effective diffusion coefficients for two polystyrene samples with different relative molecular weights of 1000 and 100,000 in cyclohexane on bone-like hydroxyapatite were found to be 5.92×10^{-17} and 6.54×10^{-17} cm^2/s, respectively. It was further confirmed that the binary effective diffusion coefficients revealed much lower values than the binary bulk ones due to the strong influence of hindered diffusion in hydroxyapatite pore network.

This work demonstrates that both Graham's diffusion cell for gaseous systems and inverse liquid chromatography technique for liquids can be successfully utilized for complex characterization of the transport properties of the novel biocompatible materials and moreover,for obtainingof transport characteristics which have beenmissing in literature.

Acknowledgments

The financial support of Grant Agency of the Czech Republic (project no. P106/11/P459) and Ministry of Education, Youth and Sports of the Czech Republic (project no. 7AMB12FR029) is gratefully acknowledged.

References:

[1] M.H. Fathi, A. Hanifi, V. Mortazavi, Preparation and Bioactivity Evaluation of Bone-Like Hydroxyapatite Nanopowder, *Journal of Materials Processing Technology*, Vol. 202, 2008, pp. 536–542.

[2] S. Agarwal, J.H. Wendorff, A. Greiner, Use of Electrospinning Technique for Biomedical Applications, *Polymer*, Vol. 49, 2008, pp. 5603–5621.

[3] F.V. Anghelina, D.N. Ungureanu, V. Bratu, I.N. Popescu, C.O. Rusanescu, Fine Structure Analysis of Biocompatible Ceramic Materials Based Hydroxyapatite and Metallic Biomaterials 316L, *Applied Surface Science*, Vol. 285, 2013, pp. 65–71.

[4] S. Ramakrishna, K. Fujihara, W.-E. Teo, T.-C. Lim, Z. Ma, *An Introduction to Electrospinning and Nanofibers*, World Scientific Publishing, 2005.

[5] E. Wicke, R. Kallenbach, Die Oberächen Diffusion von Kohlendioxyd in Aktiven Kohlen, *Kolloid Zeitschrift*, Vol. 97, 1941, pp. 135–151.

[6] T. Ackmann, L.G.J. de Haart, W. Lehnert, D. Stolten, Modeling of Mass and Heat Transport in Planar Substrate Type SOFCs, *Journal of The Electrochemical Society*, Vol. 150, 2003, pp. 783–789.

[7] J. Gutenwik, B. Nilsson, A. Axelsson, Determination of Protein Diffusion Coefficients in Agarose Gel with a Diffusion Cell, *Biochemical Engineering Science*, Vol. 19, 2004, pp. 1–7.

[8] K. Soukup, P. Schneider, O. Šolcová, Comparison of Wicke-Kallenbach and Graham's Diffusion Cells for Obtaining Transport Characteristics of Porous Solids, *Chemical Engineering Science*, Vol. 63, 2008, pp. 1003–1011.

[9] K. Soukup, P. Schneider, O. Šolcová, Wicke-Kallenbach and Graham's Diffusion Cells; Limits of Application for Low Surface Area Porous Solids, *Chemical Engineering Science*, Vol. 63, 2008, pp. 4490–4493.

[10] J. Valuš, P. Schneider, A novel Cell for Gas Counter-Diffusion Measurements in Porous Pellets, *Applied Catalysis*, Vol. 1, 1981, pp. 355–366.

[11] D.S. Scott, W. Lee, J. Papa, The Measurement of Transport Coefficients in Gas-Solid Heterogeneous Reactions, *Chemical Engineering Science*, Vol. 29, 1974, pp. 2155–2167.

[12] P. Schneider, Multicomponent Isothermal Diffusion and Forced Flow of Gases in Capillaries. *Chemical Engineering Science*, Vol. 33, 1978, pp. 1311–1319.

[13] M. Kubín, Beitrag zur Theorie der Chromatographie, *Collection of Czechoslovak Chemical Communications*, Vol. 30, 1965, pp. 1104–1118.

[14] E. Kučera, Contribution of the Theory of Chromatography: Linear Non-Equilibrium

Elution Chromatography, *Journal of Chromatography*, Vol. 19, 1965, pp. 237–248.
[15] V. Hejtmánek, P. Schneider, Diffusion of Large Molecules in Porous Glass, *Chemical Engineering Science*, Vol. 49, 1994, pp. 2575–2584.
[16] L.J. Fetters, N. Hadjichristidis, J.S. Lindner, J.W. Mays, Molecular Weight Dependence of Hydrodynamic and Thermodynamic Properties for Well-Defined Linear Polymers in Solution, *Journal of Physical and Chemical Reference Data*, Vol. 23, 1994, pp. 619–640.
[17] I.A. Kathawalla, J.L. Anderson, Pore Size Effects on Diffusion of Polystyrene in Dilute Solution, *Industrial & Engineering Chemistry Research*, Vol. 27, 866–871.